actuators

MDPI

Article

The Design and Application of a Vectored Thruster for a Negative Lift-Shaped AUV

Hong Zhu [1], Lunyang Lin [1,2], Chunliang Yu [1], Yuxiang Chen [1,*], Hong Xiong [1], Yiyang Xing [1] and Guodong Zheng [1]

[1] Institute of Deep-Sea Science and Engineering, Chinese Academy of Sciences, Sanya 572000, China; zhuh@idsse.ac.cn (H.Z.); linly@idsse.ac.cn (L.L.); yucl@idsse.ac.cn (C.Y.); xiongh@idsse.ac.cn (H.X.); xingyy@idsse.ac.cn (Y.X.); zhenggd@idsse.ac.cn (G.Z.)
[2] University of Chinese Academy of Sciences, Beijing 100049, China
* Correspondence: chenyux@idsse.ac.cn

Abstract: Autonomous underwater vehicles (AUVs), as primary platforms, have significantly contributed to underwater surveys in scientific and military fields. Enhancing the maneuverability of autonomous underwater vehicles is crucial to their development. This study presents a novel vectored thruster and an optimized blade design approach to meet the design requirements of a specially shaped AUV. Determining the ideal blade characteristics involves selecting a maximum diameter of 0.18 m and configuring the number of blades to be four. Furthermore, the blades of the AUV were set to rotate at a speed of 1400 revolutions per minute (RPM). The kinematics of the thrust-vectoring mechanism was theoretically analyzed. A propulsive force test of the vectored thruster with ductless and ducted propellers was performed to evaluate its performance. A ductless propeller without an annular wing had a higher propulsive efficiency with a maximum thrust of 115 N. Open-loop control was applied to an AUV in a water tank, exhibiting a maximum velocity of 0.98 m/s and a pitch angle of 53°. The maximum rate of heading angle was 14.26°/s. The test results demonstrate that the specially designed thrust-vectoring mechanism notably enhances the effectiveness of AUVs at low forward speeds. In addition, tests conducted in offshore waters for depth and heading control validated the vectored thruster's capability to fulfill the AUV's motion control requirements.

Keywords: autonomous underwater vehicles; novel vectored thruster; thrust-vectoring mechanism; specially shaped AUV

Citation: Zhu, H.; Lin, L.; Yu, C.; Chen, Y.; Xiong, H.; Xing, Y.; Zheng, G. The Design and Application of a Vectored Thruster for a Negative Lift-Shaped AUV. *Actuators* **2024**, *13*, 228. https://doi.org/10.3390/act13060228

Academic Editor: Keigo Watanabe

Received: 14 May 2024
Revised: 11 June 2024
Accepted: 16 June 2024
Published: 19 June 2024

1. Introduction

As an extremely significant tool, underwater vehicles play a significant role in various ocean-related activities, such as military applications, scientific research, port operations, and maritime safety. Underwater vehicles are primarily used for inaccessible, hazardous, and expensive tasks for divers [1]. Engineers have an essential mission to improve the capability of underwater vehicles to explore oceans while performing these tasks [2].

These missions require underwater vehicles equipped with advanced and vital technologies to expand their capabilities such as maneuvering and autonomy. Sophisticated sensors and intelligent algorithms can improve the autonomy of underwater vehicles. The propulsion system is a crucial factor determining the maneuverability of underwater vehicles; hence, the question of how to incorporate underwater propulsion technology with high navigation efficiency and excellent maneuverability has always been a research focus in the field of underwater robots [3].

Different missions and applications determine the shapes, configurations, and propulsion systems of underwater vehicles [4]. The propulsion systems of underwater vehicles can be classified into three types: classical rear propeller propulsion, bio-inspired propulsion [5,6], and vectored thrust propulsion [1]. The propulsion strategy of an underwater vehicle determines its movement-control mode. Underwater vehicles intended for

high-speed cruising are designed with streamlined hulls to reduce hydrodynamic drag. A main propeller equipped at the tail cone enables these streamlined-shaped vehicles to propel, and the steering ability is achieved by changing the angle of fins and rudders [7]. However, a major disadvantage of propulsion technology is that the underwater vehicle control authority is unstable at low speeds or suspended [8]. Under such conditions, the effectiveness of fins and rudders for controlling the vehicle is diminished or rendered nearly ineffective.

However, this limitation can be overcome by adding additional thrusters to underwater vehicles [9,10]. The ineffectiveness of the control surfaces was solved using the differential propulsive forces of the thrusters. This results in an overall hull configuration of the underwater vehicle complex. The weight, manufacturing cost, hydrodynamic drag, and energy consumption of underwater vehicles have also increased [11].

Another effective method to overcome the drawbacks discussed above is vectored thrust propulsion (VT), which replaces conventional rear or multiple propeller propulsion and bio-inspired propulsion [7]. Typically, an underwater vehicle is equipped with only one vectored thruster. The vectored thrust provided by the vectored thruster can be decomposed into two components: a control force and a driving force.

In recent decades, the application of vector propulsion technology in the field of underwater robots has undergone rapid development. There are relevant studies documenting the application of vector propellers in various underwater robots. However, some vector propellers remain at the theoretical design stage or prototype verification stage. In other words, during the process of transforming vectored thruster prototypes into practical applications, a multitude of issues tend to become pronounced. The following will introduce the design or applications of typical vector propellers.

Some vector propulsion technologies have their main propulsion motor placed at the end of the propeller, and the propeller is directly driven by a waterproof motor, meaning that the motor is exposed to water. The vector mechanism changes the thrust direction by altering the orientation of the motor itself. Obviously, this kind of mechanism has a large rotational inertia at its end, and when the propeller deflects, the power required by the reversing drive motor is also relatively large. Below, we will introduce several vector propellers of this type.

The Bluefin series AUV [12] is equipped with a vector propulsion system that changes the orientation of the mobile platform through the linear movement of a push rod to alter the direction of the propeller thrust. This vector propulsion device boasts a simple mechanical structure, flexible movement, and easy sealing.

The vectored thruster designed by E. Cavallo consists of a spherical parallel mechanism, which comprises a fixed platform and a moving platform connected by three identical chains [13,14]. By rotating the three active joints on the fixed platform, it drives the rotation of the three driven joints connected to the moving platform, thereby changing the attitude of the moving platform.

Spherical underwater robots employ three or four vectored thrusters based on pumped-water jets, with each vectored thruster controlled by two servo motors for a total of 2 DOFs (degrees of freedom) [11,15]. This vector mechanism is only suitable for this kind of small underwater robot like SUR-I and SUR-III. This article refers to this design method, but there have been critical issues in practical applications, which will be discussed later in the text.

For AUVs with a torpedo shape and limited tail space, Tao Liu designed a vector mechanism based on the 3-RPS parallel mechanism. The author conducted simulations on this mechanism but did not provide any practical application cases. Compared to the method of using two servo motors to achieve two degrees of freedom, this mechanism utilizes three linear motors. The control of various kinematic and dynamic methods for this mechanism is overly complex, and there are few documented cases of its actual application in AUVs. The biggest issue is that for the three linear motors of this mechanism to achieve

a certain angle of the vectored thruster, a certain response time is required, resulting in input time delays for the AUV [2,7].

In addition to the direct drive of the propeller by a waterproof motor, there are also some vector propellers that utilize a non-waterproof motor to drive the propeller through a drive shaft or magnetic coupling. The drive shaft is a flexible transmission shaft formed by connecting a ball gear and a universal joint in series. The propeller is rotated in different thrust directions by driving the flexible shaft with the main motor. The magnetic coupling drive method achieves the rotation of the propeller in different thrust directions through a magnetic coupling drive.

A study has reported the implementation of a spherical reconfigurable magnetic coupling (S-RMC) method for motor-driven propellers [16]. A servo motor is utilized to ensure that the change in thrust direction can be achieved with one degree of freedom (DOF). However, the vectored thruster remains in the design phase and has not been applied to underwater robots.

Based on reference [16], which utilized a single steering gear to achieve one degree of freedom for the vectored thruster, Yaxin Li et al. [3] proposed the use of two servo motors to form a vector steering actuator, enabling two degrees of freedom for the vectored thruster. To achieve spatial vector thrust output, the steering actuator is assembled from two intersecting arc-shaped slide rails. At the end of each slide rail, a servo motor is mounted on the support frame to change the deflection angle. The propeller's driving method still utilizes the spherical reconfigurable magnetic coupling (S-RMC) approach.

Luca Pugi and his team proposed a method similar to the one in reference [16] for designing a vectored thruster. To address the sealing issue, this vectored thruster employs two magnetic couplings. One magnetic coupling is used by the main motor to drive the propeller rotation, while the other magnetic coupling is used by the steering gear to adjust the attitude of the thruster, thus achieving one degree of freedom for this vectored thruster [8]. It has not been actually applied to underwater robots.

The magnetic coupling-based vector propulsion device scheme is conducive to achieving the sealing of the main motor, but the non-collinear torque transmission performance of the magnetic coupling shaft coupler will deteriorate when the propeller deflects.

There are also some studies that provide cases of propeller rotation driven by the combination of drive motors, spherical gears, and transmission shafts [17]. For instance, the gear-and-ring vector propulsion device developed by MIT [18] utilizes gears meshed with incomplete gear rings to control the horizontal and vertical movement of the propeller. This solution is still in the theoretical research stage.

In conclusion, a considerable amount of research is currently focused on underwater vector propellers. While there are mature design schemes for vector propellers with classic application cases, most of the research is still in the model testing phase, and practical applications are not yet mature. The main reasons for this inability to achieve practical application are poor sealing reliability, as well as corrosion issues faced by mechanisms in seawater; the non-collinearity of the propeller shaft and motor shaft during deflection, which can easily lead to low transmission efficiency; complex vector mechanisms prone to processing errors, reduced coupling between branches, and increased control difficulty; and the cumulative errors of each joint in serial vector mechanisms, which can result in low deflection accuracy at the end.

There is a comprehensive plan available as a reference for designing an underwater propeller prototype. The design of the propeller prototype typically requires considerations of the driving motor, the shape and diameter of the propeller, the number of blades, the shape of the duct or nozzle, the drive circuit, and the coupling transmission components [19,20]. After the design is completed, the thrust, friction, torque, and efficiency values of the propeller are first calculated through finite element analysis [21]. Secondly, an open-water test is conducted to identify the thruster parameters [22]. Finally, performance tests are carried out on an actual underwater vehicle to verify the performance of the propeller [23].

The main contribution of this study lies in the design of two prototype vectored thrusters based on linear actuators and steering motors, which aim to fulfill the design requirements of specially shaped AUV. Both vectored thrusters were utilized for AUVs to perform underwater missions lasting for weeks and months, and the linear actuator-based vectored thruster was selected after evaluation. Propulsion force tests were conducted to evaluate the performance of the vectored thruster, and kinematic analysis was performed on the thrust-vectoring mechanism to achieve reliable and precise control. To verify the design principles, an AUV equipped with this vectored thruster was tested in a water tank. Different thrust forces for propelling the AUV were tested to investigate the vehicle's open-loop response at various vector angles. Additionally, the closed-loop control performance of the vectored thruster was tested in a real marine environment. Experimental results demonstrate that the thrust-vectoring mechanism can adjust the vector thrust in a directionally, and the vectored thruster can achieve a sufficient level to meet the control requirements of the AUV.

This study focuses on the design and validation of a novel vectored thruster that exhibits reliable performance and precise control. Successfully applied to the motion control of AUV, it provides a new solution for enhancing the design and performance of AUV. Section 2 presents the design requirements of the vectored thruster, and the general design of the vectored thruster is analyzed. In Section 3, the kinematics of the thrust-vectoring mechanism are discussed and the propulsive force test of the vectored thruster is described. Section 4 conducts water tank tests and offshore depth and heading control tests using an actual AUV to verify the performance of the developed prototype. Finally, Section 5 summarizes the study and discusses future work.

2. The General Design of the Vectored Thruster

2.1. Specifications of the Solar-Powered AUV

As illustrated in Figure 1, an underwater vehicle preparing to install the designed vectored thrust is a specially shaped AUV. The required design parameters for the AUV are listed in Tables 1 and 2.

Figure 1. A specially shaped AUV equipped with a vectored thruster.

Table 1. Main parameters of AUV.

Parameter	Value
Weight	205 kg
Dimension	2391 mm × 2130 mm × 519 mm
Max. speed	2.5 kn
Designed positive buoyancy	1 kg

Table 2. The relationship between power and speed of AUV.

Parameter	Value			
V (knots)	1	1.5	2	2.5
P_E (W)	8.12	24.76	56.93	109.74
P_E (hp)	0.0107	0.0328	0.0753	0.1452
R (N)	15.79	32.09	55.33	85.33

The designed vectored thruster was installed below the stern of the AUV. The AUV was not equipped with traditional fins or rudders. The driving and control forces generated by the vectored thruster combine to form the resultant force for controlling the motion of the AUV. The inclination of the thruster is a critical variable that governs the operational efficacy of the AUV. The deflection angle of the vectored thruster determines the direction and magnitude of the driving and control force.

The design of a vectored thruster consists of two parts. The first part involves the design of the thruster itself, including the selection of the motor and the design of the propeller. The second part is the vector mechanism that enables the spatial vector output of the thruster, typically with two degrees of freedom. This study first designed the corresponding propeller based on the motor specifications, and then designed and fabricated two types of vector mechanisms using steering motors and linear motors. Finally, open-water tests of the thruster and control tests of the autonomous underwater vehicle (AUV) were conducted to verify the practical application performance of the vectored thruster.

2.2. Design of Propeller Blades

The design of underwater propeller blades requires comprehensive consideration of various factors, including blade shape, angle, pitch, rotational speed, noise and vibration, load, and strength, as well as material and manufacturing processes. These factors interact with each other and jointly determine the performance and service life of the propeller. In this study, the underwater D5085 motor was selected, and the motor parameters are presented in Table 3. To ensure that the propeller and motor can work efficiently and stably together to achieve the best propulsion effect, the matching relationship between the underwater propeller blade and the motor must be fully considered during the design process.

Table 3. The parameters of the motor.

Parameter	Specification
Product Model	D5085
Voltage	22.2 V
No-load Current	0.8 A
No-Load Speed	3100 rpm
Load Current	29.5 A
Power	650 W
Weight	680 g

To meet the design requirements of an AUV in Table 1, an analysis of the propeller design was conducted, including variations in the number of blades and propeller diameters. This investigation was conducted within the framework of an optimum blade design technique. The present study considered two, three, and four blades. The diameter values for the propeller were in the range of 0.15~0.18 m. The other relevant parameters for the propeller are listed in Table 4.

Table 4. The parameters of the propeller.

Parameter	Specification
Airfoil Profile	NACA
Number of Blades	2–4
Number of Propeller	Single
Propeller Rotation Direction	Clockwise
Diameter of Blade	0.15~0.18 m
Pivot Diameter	0.058 m
Rotate Speed of the Propeller	400 r/min~1600 r/min

The propulsion efficiency was calculated for different rotational speeds, diameters, and number of blades to obtain the optimum combination. The values of the rotation speeds were in the range of 400–1600 rpm. Two, three, or four blades were used. The calculation results are shown below.

As shown in Figure 2, the larger the diameter of the blade, the higher the efficiency. When the maximum diameter of the blade was 0.18 m, the propulsion efficiency of the propellers with different numbers of blades did not differ significantly. Therefore, the number of blades of the propeller was set to four. When the rotation speed was 1400 rpm, the propulsion efficiency was the highest, and in the range of 1000–1600 rpm, the propulsion efficiency was also relatively high. Considering the motor's efficiency, the propeller speed was selected as 800–1600 rpm. A preliminary determination of the propeller parameters was obtained, which is shown in Table 5.

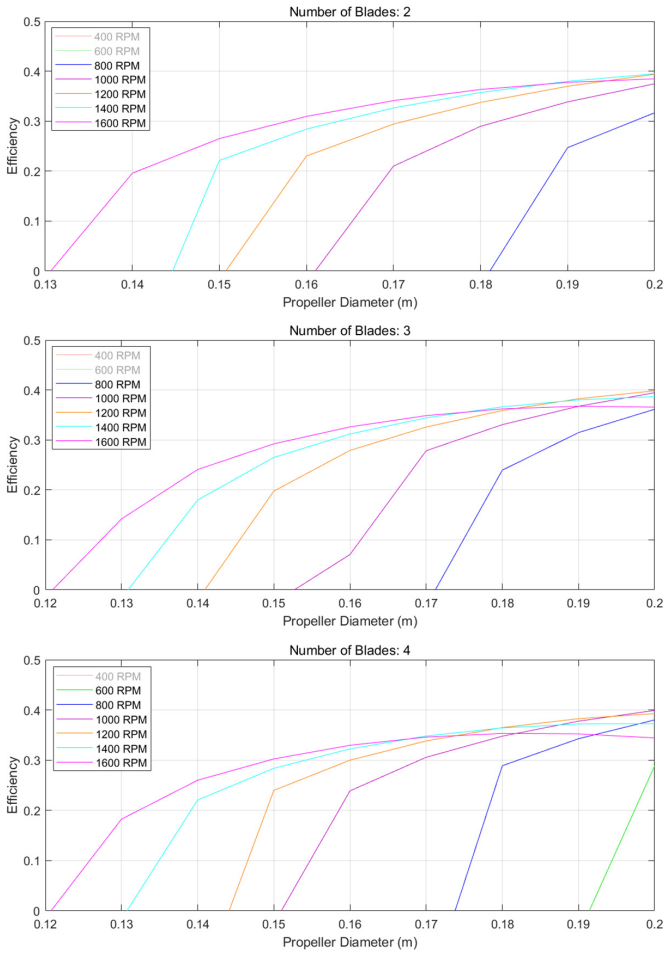

Figure 2. Optimization results of rotation speed, blade number, and diameter.

Table 5. The preliminary parameters of the propeller.

Parameter	Specification
Airfoil Profile	NACA
Number of Blades	4
Diameter of Blade	0.18 m
Rotate Speed of the Propeller	800 r/min~1600 r/min

For a rotational speed that meets the thrust requirements, the Lifting Line Theory is used to optimize the chord length of the propeller and the torque, M_{Prop}, generated by the optimized chord length of the propeller at a specific speed. We assumed that the torque generated by the motor was M_{motor}. Considering the torque loss due to sealing, friction, and other reasons for the motor, the efficiency of the motor was set to $M_{motor} = 0.8 \cdot M_{Prop}$. The blade design employed the foil NACA65A010 thickness distribution, with a modified mean line of NACA a = 0.8 modified mean line.

Load coefficient, σ_{T0}, is defined as

$$\sigma_{T0} = \frac{T}{\frac{1}{2}\rho\pi R^2 V_a^2} \tag{1}$$

The efficiency formula, η_{disk}, for an ideal actuating disc is

$$\eta_{disk} = \frac{2}{1 + \sqrt{1 + \sigma_T}} \tag{2}$$

Classical propeller open-water characteristics were used as the performance metrics in this study. The metrics were the thrust coefficients K_T, torque coefficient K_Q, propeller efficiency J, efficiency η, propeller speed n, and diameter of blade D.

$$K_T = \frac{T}{\rho n^2 D^4} \tag{3}$$

$$K_Q = \frac{Q}{\rho n^2 D^5} \tag{4}$$

$$J = \frac{V_a}{nD} \tag{5}$$

$$\eta = \frac{K_T}{K_Q}\frac{J}{\pi} \tag{6}$$

The propulsion coefficients K_{T0} and K_{T1} were used to represent the load coefficients σ_{T0} and σ_{T1}. The advance ratios were taken across the range of 0.14 to 0.34. Under the condition of satisfying the thrust coefficient, the propeller design was optimized for different advance ratios. Finally, the relationship between K_{T0} and K_{T1}, as well as the open-water performance curve K_T and the efficiency of the propeller under different design inlet ratios, were obtained, as shown in Figure 3.

The open-water characteristic curves of K_T, K_Q, and η based on the designed blade are shown in Figure 4.

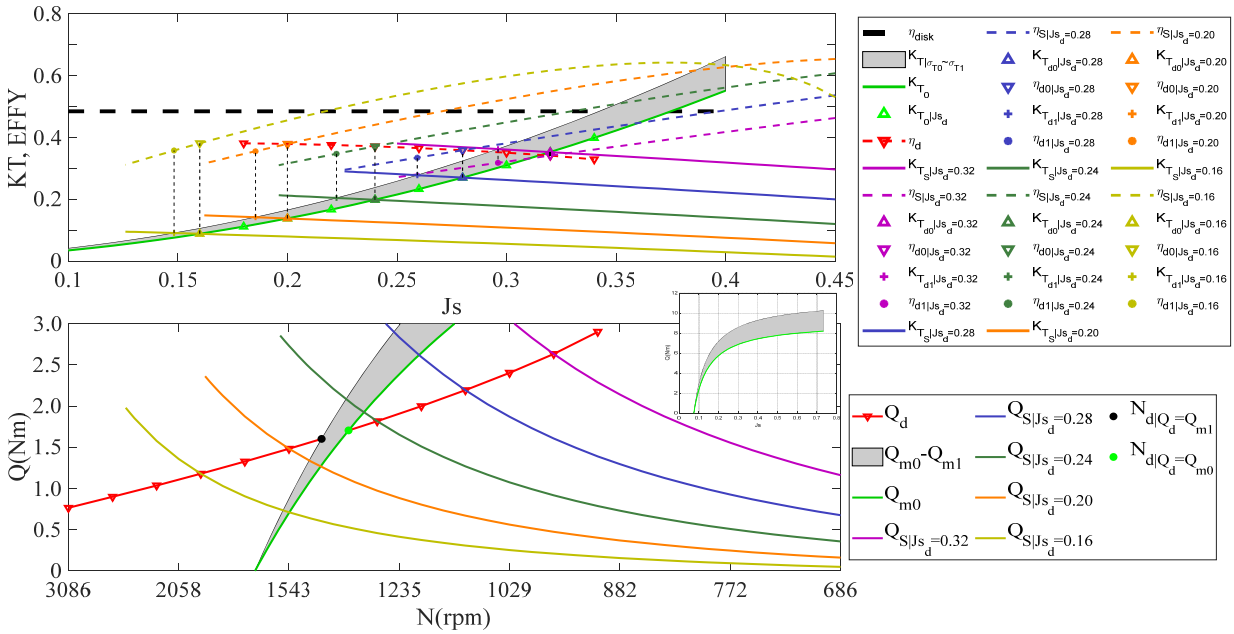

Figure 3. Thrust-torque balance propeller design points and performance curves.

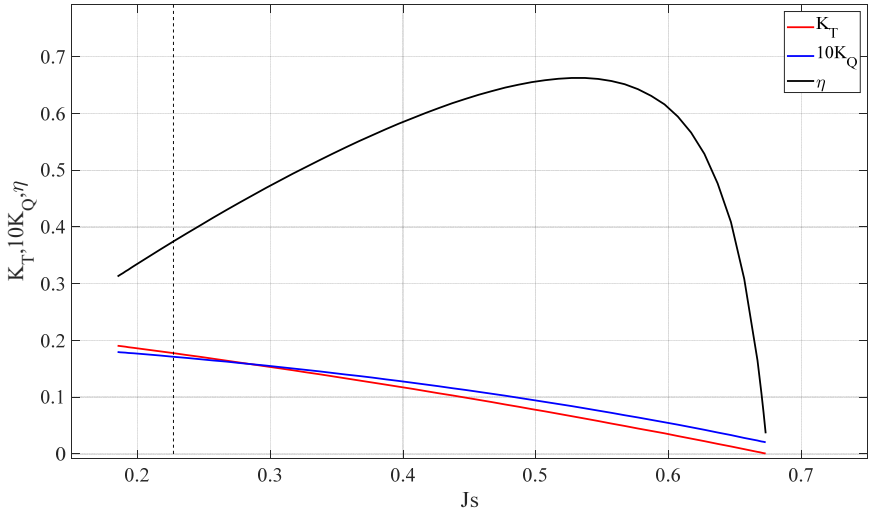

Figure 4. Open-water characteristic curves.

2.3. Performance Testing of the Thrust-Vectoring Mechanism

After summarizing the relevant literature on the design of vectored thrusters, it can be seen that there are two types of vector mechanisms used to achieve the spatial movement of thrusters: steering motors and linear motors. In this study, two types of vectored thrusters were designed and manufactured, as shown in Figure 5.

The vectored thruster in Figure 5a was designed with reference to the vectored thrusters used in the small underwater robots SUR-I and SUR-III, which utilize two steering motors to achieve two degrees of freedom of rotation of the vectored thruster. Steering motor 1 enables the rotation of the thruster around the x-axis with a range of [−180°, 180°], while steering motor 2 achieves rotation around the y-axis within a range of [−20°, 20°]. The significant advantage of this approach lies in its simple structural design, and the steering motors' faster response speed compared to linear actuators. Standard steering motors typically take from 0.11 s to 0.21 s to rotate 60°, which can be considered almost instantaneous for the motion control of AUVs with slower movement speeds.

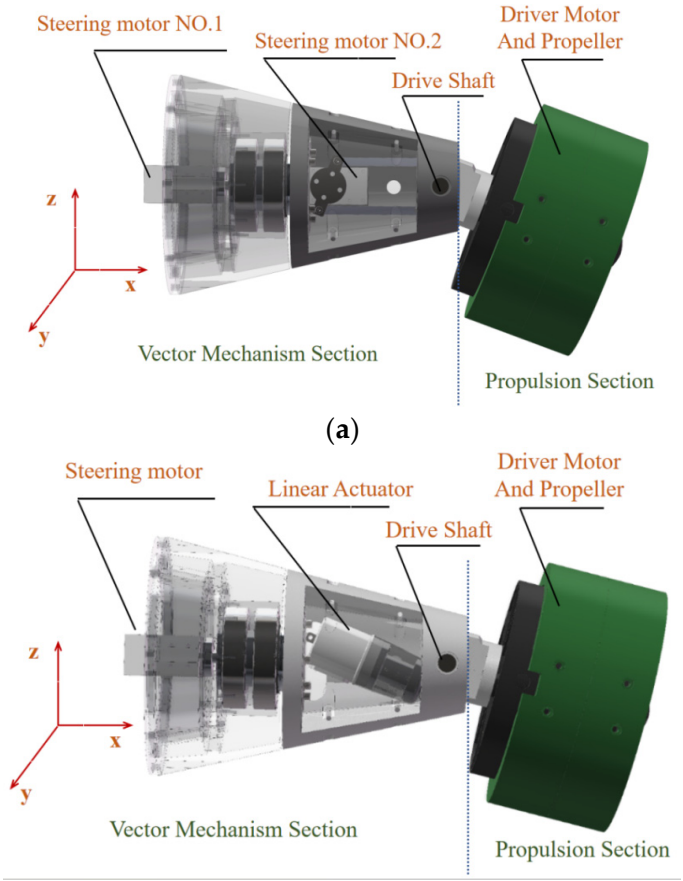

Figure 5. Schematic of vectored thruster configuration. (**a**) Two steering motors; (**b**) a steering motor and a linear actuator.

When this vector mechanism is applied to an AUV, the circular duct of the thruster functions as a rudder surface. As steering motor 2 rotates around the y-axis up and down, the greater rotation speed generates higher resistance. Figure 6 shows the vector diagram of the surface pressure field of the AUV operating at speeds of 0.5 kn, 1 kn, and 2 kn, with a detailed vector diagram of the thruster enclosed in the red box. The surface pressure distribution of the AUV remained almost the same at these three speeds, and the regions of maximum and minimum pressure distribution were identical. The key point to note is that when the speed was 0.5 kn, 1 kn, and 2 kn, the maximum pressure at the front of the annular duct of the AUV's vectored thruster was approximately 30 Pa, 130 Pa, and 520 Pa, respectively, while the rear of the duct was under negative pressure. The pressure at the front of the circular duct was significantly greater than that at the rear, indicating that the circular duct encountered significant hydrodynamic resistance. And, the hydrodynamic resistance increased exponentially with the increase in speed, and steering motor 2 needs to provide torque equal to the hydrodynamic force to maintain the attitude of the vectored thruster. If steering motor 2 sustains a large torque for a prolonged period, it can lead to damage. When this solution was applied to an AUV for sea trials, the lifespan of steering motor 2 often lasted for only a few hours. From this, it can be concluded that steering motor-based vectored thrusters are not suitable for underwater robots.

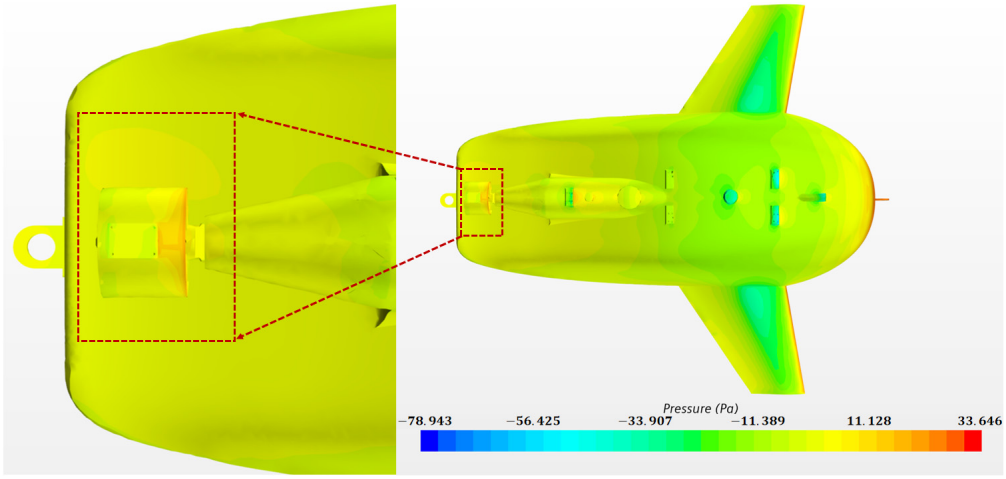

(**a**)

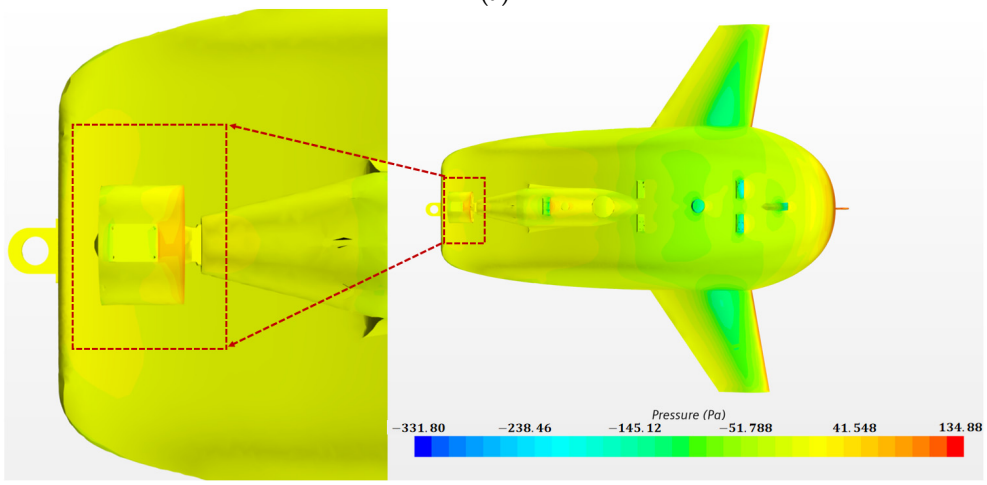

(**b**)

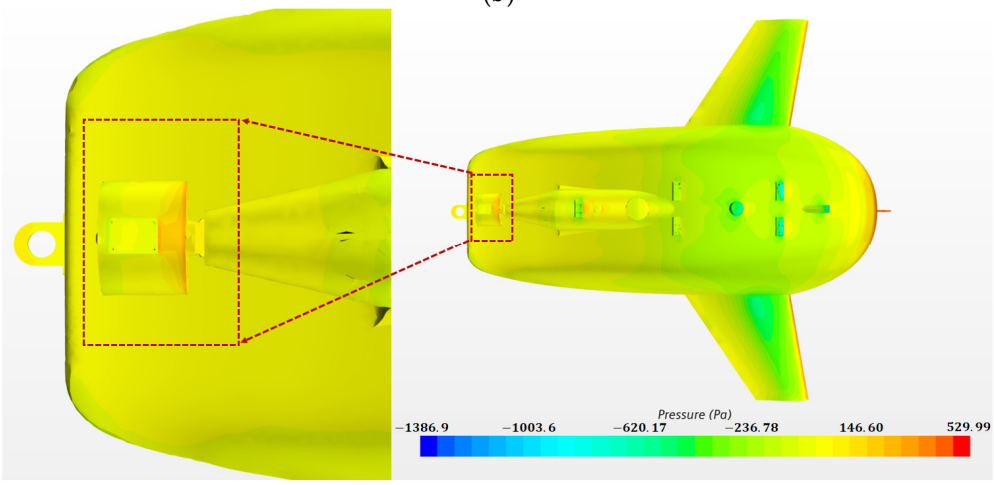

(**c**)

Figure 6. Velocity and pressure cloud maps of an AUV. (**a**) 0.5 kn; (**b**) 1 kn; and (**c**) 2 kn.

In Section 2.2, the design of the blade of the vectored thruster is described. This section discusses the vector mechanism of the vectored thruster. As shown in Figure 5, the vectored thruster designed in this work was composed of a linear actuator and a steering motor, a stepping motor, and a steering motor, which achieved a change in the tilt angle. The tilt angle combines two angles: elevation α and azimuth β. Referring to Figure 5, when the vectored thruster rotates around the y-axis, this was defined as a change in the

elevation angle α of the vectored thruster, and the red arrow indicates that the rudder is pointing downward at this moment, as shown in Figure 7a. Similarly, when the vectored thruster rotates around the x-axis, this was defined as a change in the azimuth angle β of the vectored thruster, and the red arrow indicates that the rudder is rotating clockwise at this moment, as illustrated in Figure 7c.

(**a**) (**b**) (**c**)

Figure 7. Tilt angle adjustment of vectored thruster relative to AUV: (**a**) elevation angle α; (**b**) initial position; (**c**) azimuth angle β.

Due to the frequent damage to steering motor 2, this study proposed an improved design for the vectored thruster. This design replaces steering motor 2 with a linear actuator. The vectored thruster comprises two parts: a propeller and a thrust-vectoring mechanism. The ductless propeller and ducted propeller are shown in Figure 8a,b, respectively, and their physical structure and local design details are shown in Figure 8c. A ducted propeller combines a screw propeller and annular wing. The annular wing also mitigates the threat posed by marine animals and seaweeds to screw propellers. However, a ductless propeller without an annular wing has higher propulsive efficiency, as shown in Figure 9. Underwater vehicles can quickly accelerate from zero or low speed to a predetermined speed.

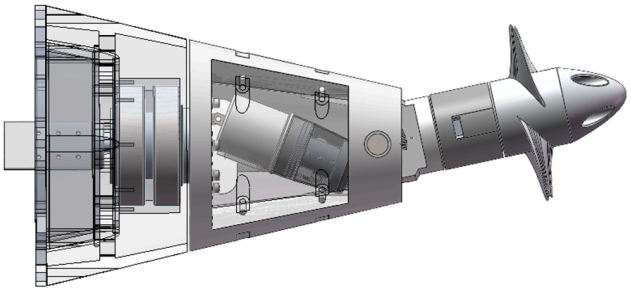

(**a**)

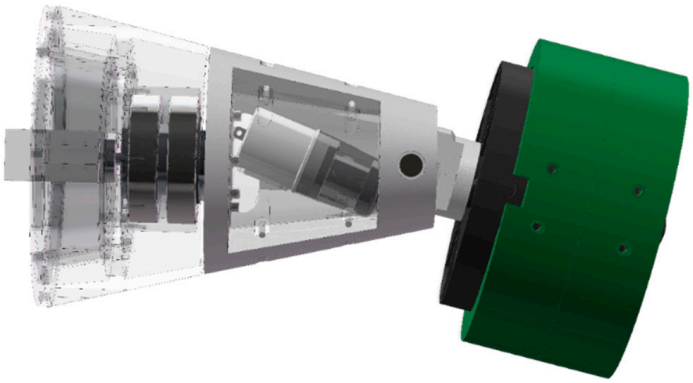

(**b**)

Figure 8. *Cont.*

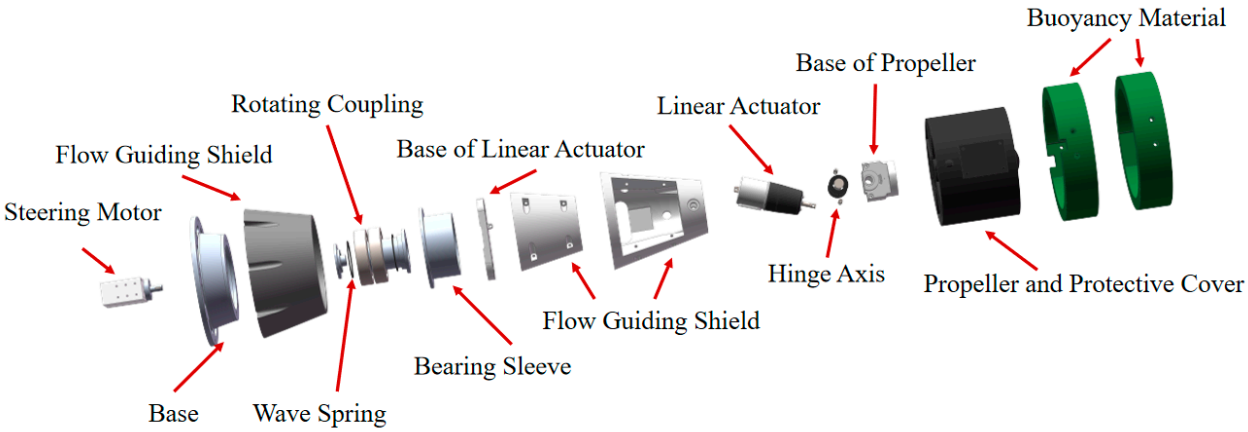

(**c**)

Figure 8. Schematic of vectored thruster configuration. (**a**) The ductless propeller; (**b**) ducted propeller; and (**c**) design details.

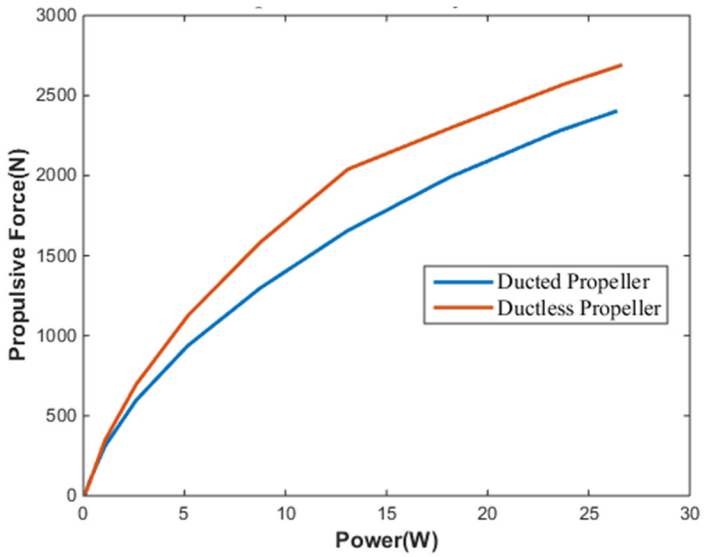

Figure 9. Thrust testing of two types of vectored thrusters.

3. Analysis and Test of the Thrust-Vectoring Mechanism

3.1. Thrust-Vectoring Mechanism Design

As an executing actuator, the vectored thruster is a critical component in the overall system of the AUV. Depending on the collocation requirements and application circumstances, there are many design schemes for the mechanical structure of thrust-vectoring mechanisms. Implementing thrust-vectoring mechanism functions for AUVs relies entirely on the chosen mechanism structure. Based on the application background of AUVs, the new design concept presented in this article for a thrust-vectoring mechanism for AUVs is shown in Figure 10.

The thrust-vectoring mechanism has two rotational degrees of freedom, which are achieved through four rotational axes. These two rotational degrees determine the spatial posture of the vectored thruster. Rotating coupling, namely rotary axis 1, joins the steering motor to a platform in a circular truncated cone, as shown in Figure 10. The steering motor can achieve platform rotation, thereby changing the azimuth angle of the vectored thruster. The platform can be considered as a fixed base relative to the ducted propeller and linear actuator.

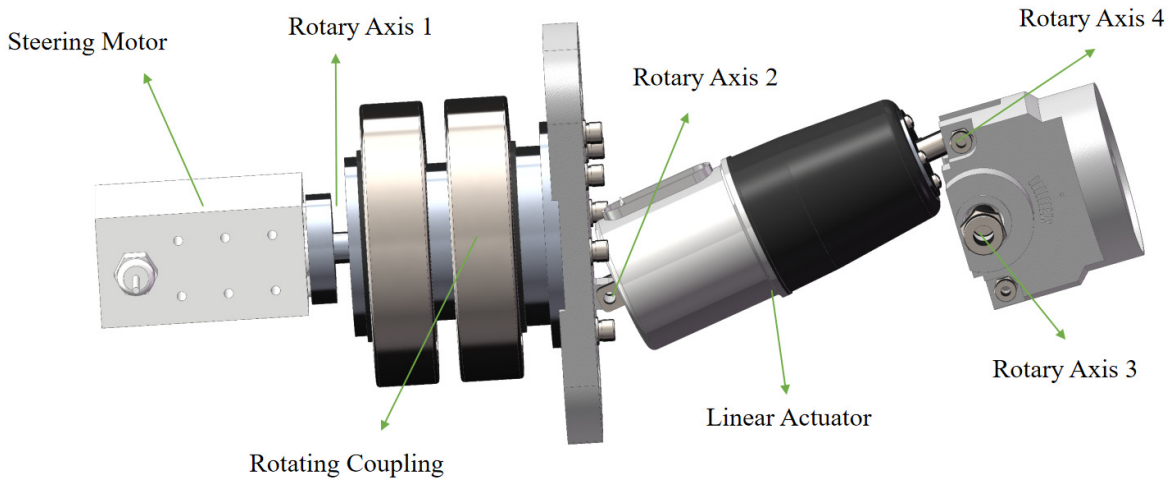

Figure 10. Thrust-vectoring mechanism.

The linear actuator assembled on a fixed platform with two joints was an actuating prismatic joint. One of the joints, rotary axis 2, was attached to the platform by a rotational joint, which had only one rotational degree of freedom. Another joint, rotary axis 4, was connected to the ducted propeller by a passive rotational joint. The linear actuator consisted of a ball screw assembly, magnet, Hall sensor, and stepping motor. The Hall sensor was installed in a fixed position inside the linear actuator, and a magnet was installed on the ball screw assembly. Thus, the feedback signal from the Hall sensor can be used to determine the operation length range of the linear actuator during working when the Hall sensor approaches the magnet. Similarly, the ductless propeller was installed on a fixed platform by a rotational joint, rotary axis 3, which had only one rotational degree of freedom. The length variation of the linear actuator achieved a rotational degree of freedom.

3.2. Kinematic Analysis of the Thrust-Vectoring Mechanism

The tilt angle of the thrust-vectoring mechanism is essential. Accurate control of the tilt angle ensures the safety and reliability of AUV operations. An accurate tilt angle measurement can be realized by mounting an attitude transducer on a fixed platform. However, this practical and straightforward approach has not been adopted because of the limited space available for the vectored thrusters. A kinematic analysis of the thrust-vectoring mechanism was performed to achieve reliable and accurate control of the tilt angle of the thrust-vectoring mechanism. This study's kinematic model of the thrust-vectoring mechanism is more accessible than the 3SPS-S parallel manipulator-based vectored thruster. There is only a linear actuator and a steering motor.

The linear actuator connected the ductless propeller and stationary platform via revolute joints. The two connecting joints are identified as points A and B. The ductless propeller was connected to the linear actuator and stationary platform by two designated connection points, points R and B, where the distance between locations A and B exhibited variability. It should be noted that points A, B, and C correspond to rotary axis 2, rotary axis 3, and rotary axis 4 in Figure 10 respectively. The distance between the RB and RA remained constant, with RB measuring 2 cm and RA measuring 10 cm, as shown in Figure 11.

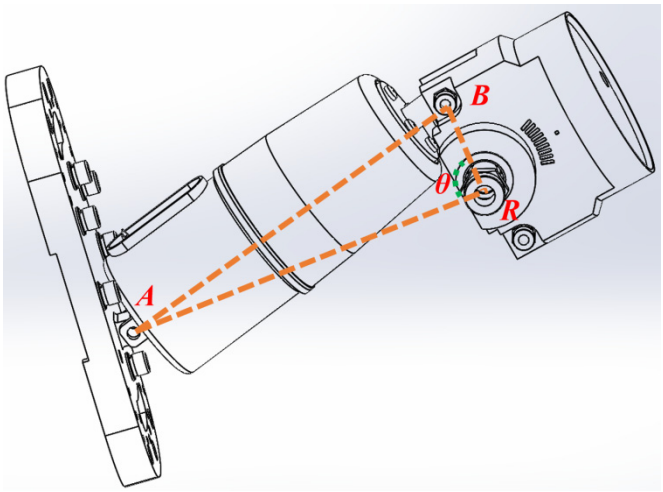

Figure 11. The schematic representation of revolute and spherical joints.

The cosine theorem describes the length of the RB, AB, and RB line segments and the angles between the neighboring line segments. The angle between RB and RA is denoted by α.

$$AB^2 = RB^2 + RA^2 + 2 \times RB \times RA \times cos(\alpha) \tag{7}$$

The relationship between the change in length of AB and α is

$$\alpha = arccos\left(\frac{RB^2 + RA^2 - AB^2}{2 \times RB \times RA}\right) \tag{8}$$

Because $RB = 2$ and $RA = 10$, the range of length changes of linear actuators is limited to

$$8 \leq AB \leq 12$$

Due to the structural limitations, the range of changes in α is limited to

$$-20^\circ \leq \alpha \leq 20^\circ$$

As shown in Figure 12, when the ductless propeller moved regularly according to the input of elevation angle α, the length changes of the linear actuator present a regular trend that echoes the inputs of elevation angle α.

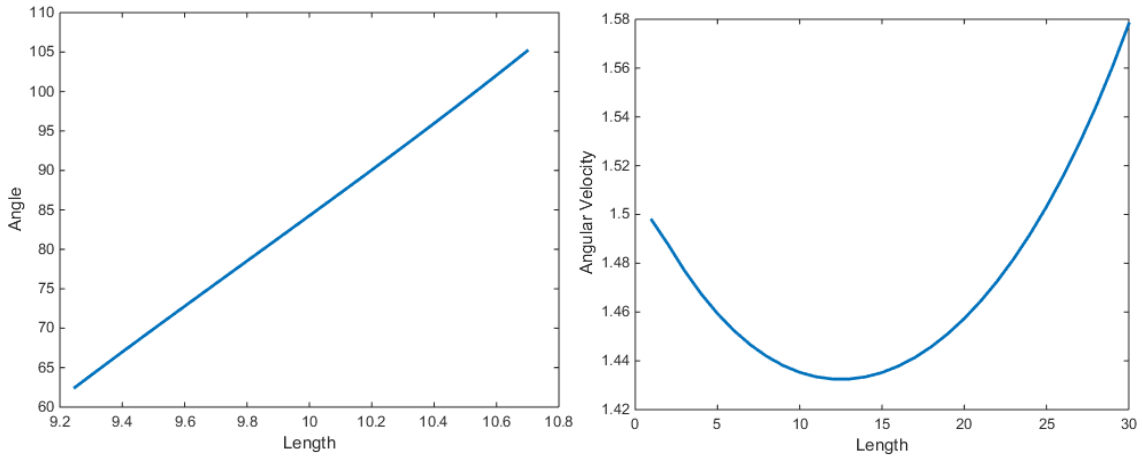

Figure 12. Changes in α, when the length of the linear actuator changes.

Thrust T in the two-dimensional plane can be rotated by adjusting the tilt angle α. The components of T are expressed as follows:

$$\begin{bmatrix} F_x \\ F_{yz} \end{bmatrix} = \begin{bmatrix} \mathrm{T}\cos\alpha \\ \mathrm{T}\sin\alpha \end{bmatrix} \tag{9}$$

β is achieved by a rotating motor, with a variation range of $[-180^\circ\ 180^\circ]$. At this time, the three components of T in three-dimensional space can be represented by the following equation:

$$\begin{bmatrix} F_x \\ F_y \\ F_z \end{bmatrix} = \begin{bmatrix} F_x \\ F_{yz} \cdot sin\beta \\ F_{yz} \cdot cos\beta \end{bmatrix} = \begin{bmatrix} \mathrm{T}\cos\alpha \\ \mathrm{T}\sin\alpha sin\beta \\ \mathrm{T}\sin\alpha cos\beta \end{bmatrix} \tag{10}$$

Assuming T is a fixed value of 112 N, the spatial motion range of the output terminal can be obtained when the sliding range of the linear actuator and steering motor are given, as shown in Figure 13.

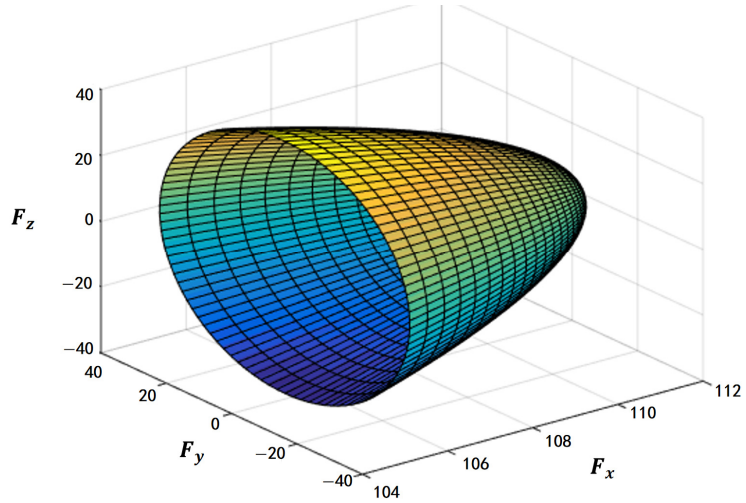

Figure 13. Propulsive surfaces of vectored thruster.

The AUV was capable of conducting six-degree-of-freedom (6DOF) movements in water, but the vectored thrusters can only control three of them, namely surge, pitch, and yaw. In this study, the component forces $\begin{bmatrix} F_x & F_y & F_z \end{bmatrix}$ for controlling the three-degree-of-freedom movement of the AUV were the outputs of PID (Proportional-Integral-Derivative) controllers. That is, given the output of the vectored thruster as $\begin{bmatrix} F_x & F_y & F_z \end{bmatrix}$, the input $\begin{bmatrix} T & \alpha & \beta \end{bmatrix}$ to the vectored thruster can be expressed using the following equation:

$$\begin{bmatrix} T \\ \alpha \\ \beta \end{bmatrix} = \begin{bmatrix} {F_x}^2 + {F_y}^2 + {F_z}^2 \\ \arctan\left(\left({F_y}^2 + {F_z}^2 \right)^{1/2} / F_x \right) \\ \arctan\left(F_y / F_z \right) \end{bmatrix} \tag{11}$$

3.3. Control of Thrust-Vectoring Mechanism

The hardware and software implementation strategies are provided in detail based on the thrust-vectoring mechanism of the AUV. The main control board used to control the vectored thruster in Figure 14a was designed by our team. The MUC is an STM32F103C8T6 chip, which is responsible for generating PWM (Pulse Width Modulation) signals to control the steering and thruster. The PWM was set at 50 Hz, with a pulse width ranging from 1 ms to 2 ms. The propeller power was the smallest when the pulse width equaled 1 ms. When the pulse width was 2 ms, the propeller power was at its maximum. The control of the linear actuator was achieved through a driver board and a position sensor. The position sensor was a Hall sensor.

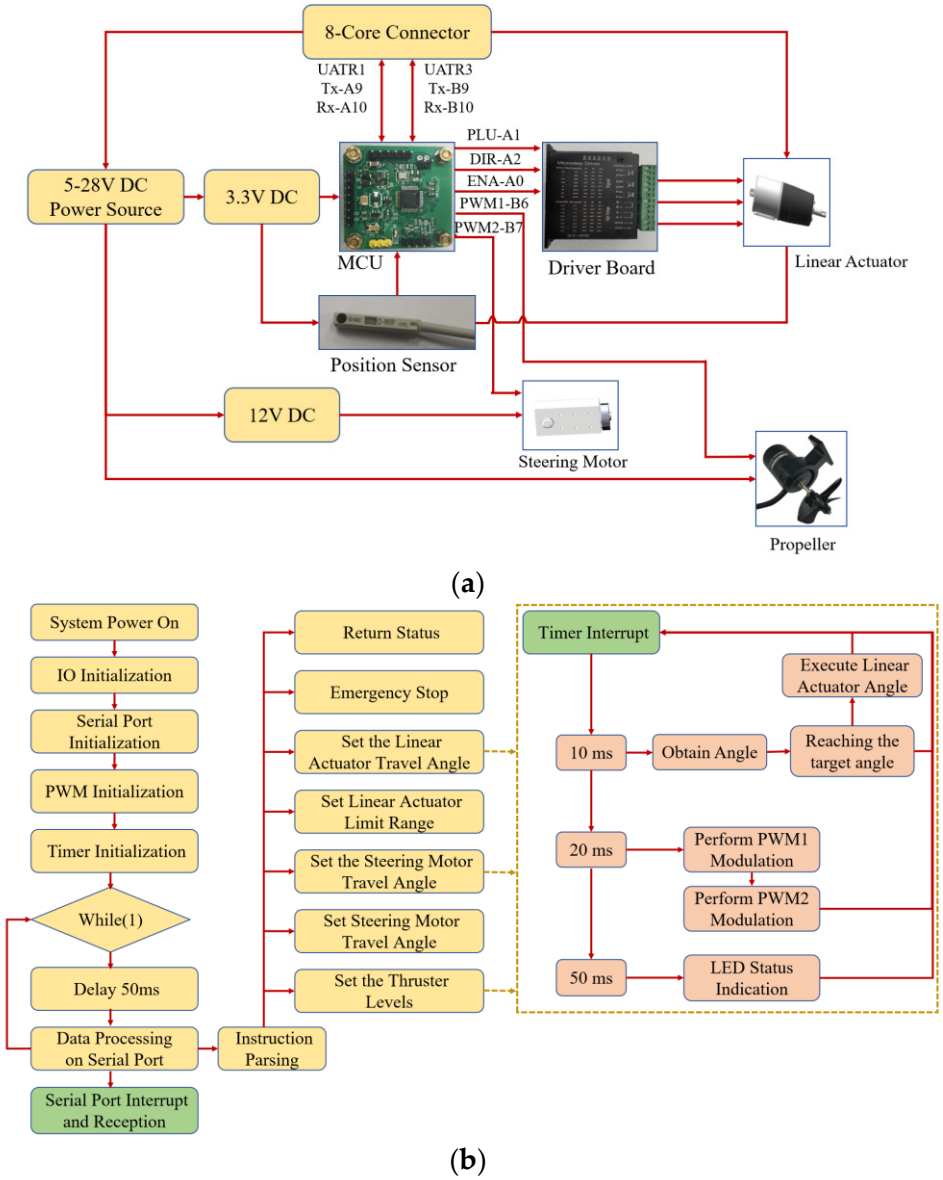

Figure 14. The (**a**) hardware and (**b**) software implementation strategies for vectored thruster.

The propeller and steering motor were controlled using PWM frequency, which was set at 50 Hz, with a pulse width ranging from 1 ms to 2 ms. The propeller power was the smallest when the pulse width equaled 1 ms. When the pulse width was 2 ms, the propeller power was at its maximum.

The relationship diagram between the propulsive force and current was obtained based on the thrust test in Section 2.3, and is shown in Figure 15a. To facilitate control of the upper computer, it was necessary to map the pulse width to the control input. The control inputs on the upper computer were set between 0 and 5. The mapping of the pulse width of 1 ms–2 ms to the control input was 0–5. The propulsive force and control inputs were fitted to obtain two curves, Fitted Curve 1 and Fitted Curve 2, as shown in Figure 15b. The control input was selected to be Level 0–4 to avoid excessive current, and the program used Fitted Curve 2 as the mapping relationship. When the pulse width was 1 ms, the control input was 0, and when the pulse width was 2 ms, the control input was 4.

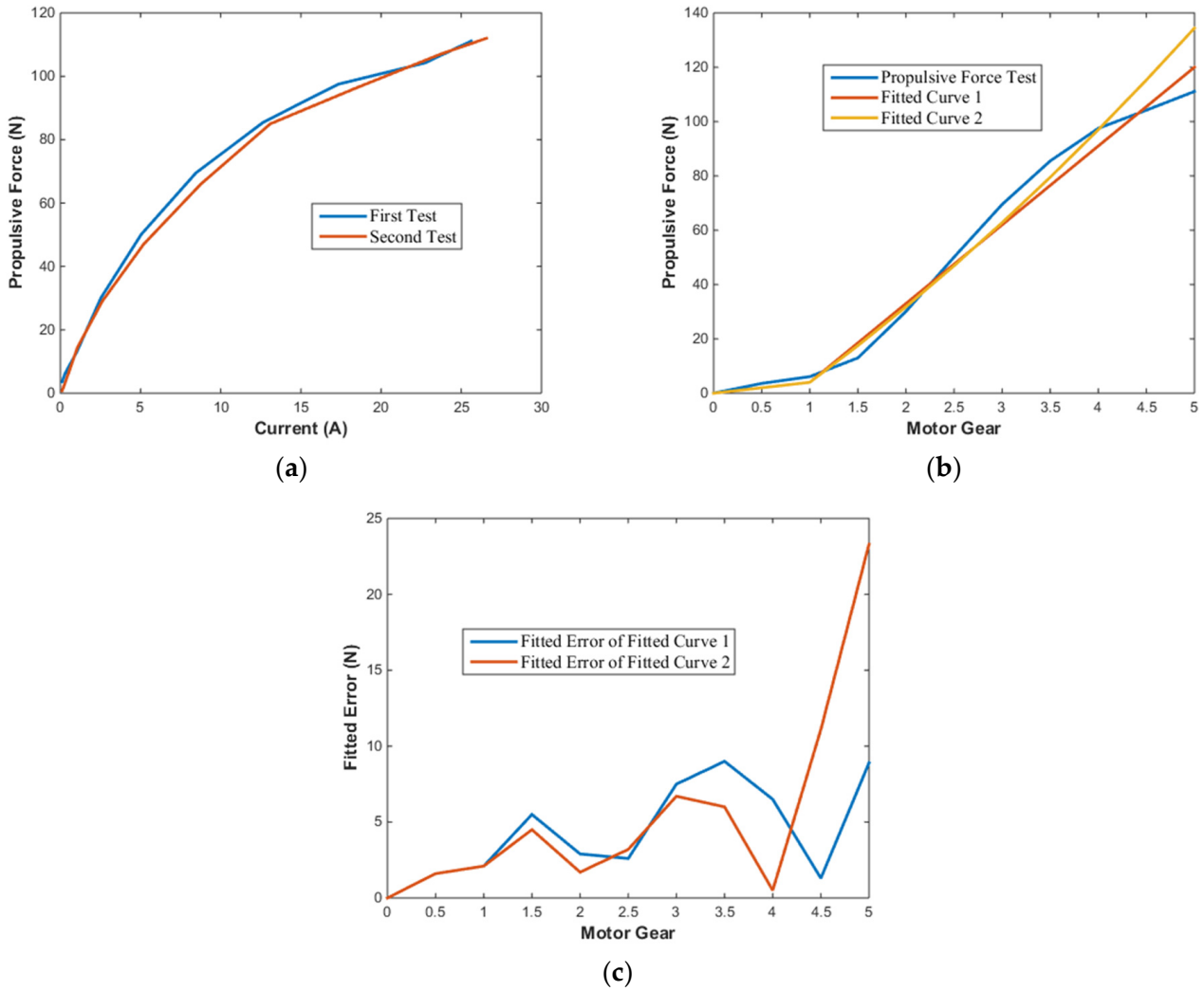

Figure 15. (**a**) Vectored thruster thrust testing; (**b**) propulsive force fitted curve; (**c**) fitting error of fitted curve.

The two curves in Figure 15c represent two types of fitted error curves. As the control input was selected as Level 0–4, the error of Fitted Curve 2 was smaller. Finally, Fitted Curve2 was selected as the mapping relationship between the pulse width and control input.

4. Field Tests and Results

Assuming that the thrust generated by the vectored thruster is T, the thrust T acting on the AUV can be illustrated as shown in Figure 16 below. Here, coordinate system $O_{NED} - X_n Y_n Z_n$ is defined as the reference inertial coordinate system, while coordinate system $O_{Body} - X_b Y_b Z_b$ is defined as the body-fixed coordinate system attached to the AUV. The thrust and its direction generated by the vectored thruster are indicated by the red arrow in the figure.

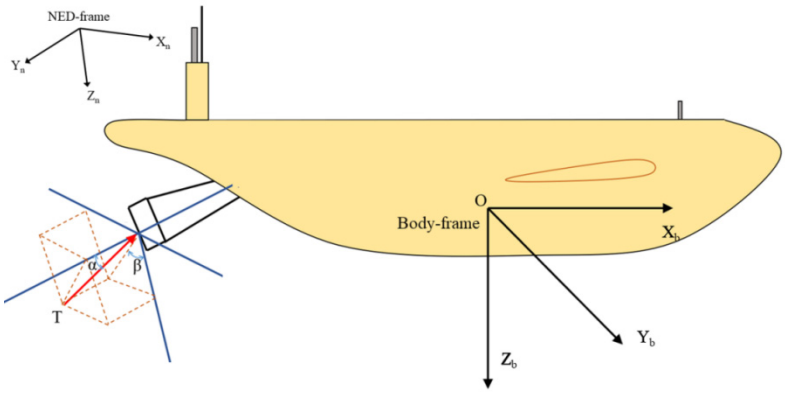

Figure 16. Coordinate frame of the AUV.

4.1. Water Tank Tests

Underwater tests of an actual AUV are necessary to determine the propulsive effect of the designed vectored thruster. A validation test was conducted in a water tank. The test environment was a water tank that was 22 m in length, 10 m in width, and 20 m in depth. The AUV was placed in an underwater environment, as shown in Figure 17, and the detailed venue and methods of the water tank tests can be found in the field test videos in the Supplementary Materials. Open-loop control for the horizontal and vertical motion of a specially shaped AUV is an essential and efficient method for evaluating the propulsive efficiency of a newly developed vectored thruster. The horizontal and vertical motions include three basic motions: surge, pitch, and yaw. The durations of the three basic motions were restricted to relatively small ranges. Surge and yaw motions were conducted in the horizontal plane, and pitch motions were conducted in the vertical plane. Owing to the asymmetric shape in the XY-plane and YZ-plane of the AUV, it was evident that the motion and hydrodynamic characteristics of the three basic motions may be distinct.

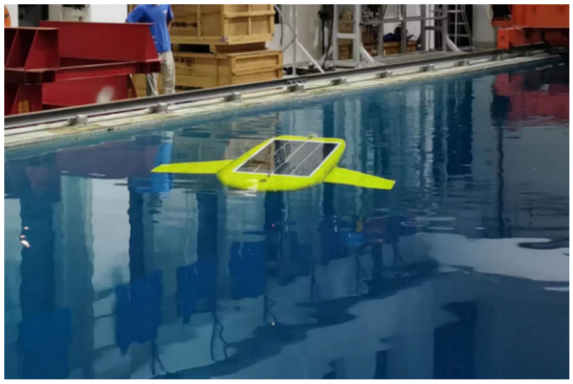

Figure 17. The AUV was tested in a water tank.

4.1.1. Surge Motion

In the surge motion, the AUV moved forward along the X-axis, and the rudder angle α and elevator angle β of the vectored thruster were equal to 0. The tests conducted were assigned to three groups, where the thrust outputs were Level 2, Level 3, and Level 4. Each test was repeated three times.

The DVL sensor measured the speed. Figure 18a–c shows the velocity–time relationship during the surge stage of the AUV. The reproducibility of the three test results was satisfactory. The maximum velocity corresponding to the three levels of propulsion inputs was 0.41 m/s, 0.65 m/s, and 0.98 m/s, respectively. Owing to the limited space in the test pool, the AUV did not accelerate to its maximum speed. The maximum speed measured did not reach the designed speed of 2.5 knots.

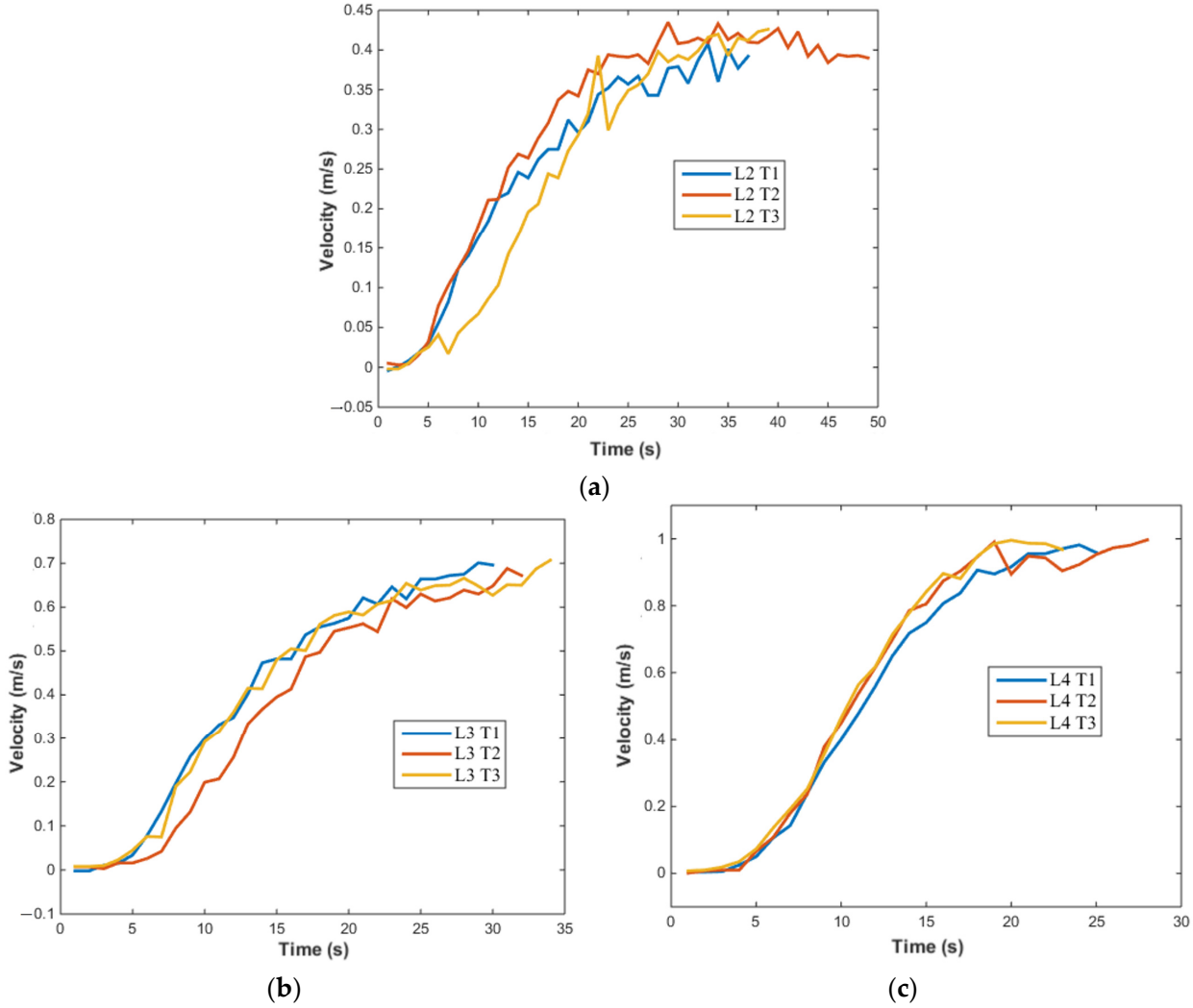

Figure 18. (**a**–**c**) Velocity–time relationship during surge motion.

4.1.2. Pitch Motion

An AUV is an underactuated underwater robot, whose depth and descent speed are related to the pitch angle. The heave motion was achieved using pitch motion. The maximum designed working depth of the AUV was 300 m. The maximum depth of the water tank was 20 m; tests of the heave motion could only be carried out in shallow water. The pitch motion was performed to verify the maximum diving speed of the AUV. To obtain the AUV's maximum pitch angle, the elevator angle α of the vectored thruster was set to a maximum angle of 20°, and the azimuth β was 0°. Simultaneously, the control input to the thrusters was fixed at 4. The test was repeated three times.

The IMU sensor was responsible for measuring the rotational angle. The depth sensor measured the depth. As Figure 19a–c indicate, the tests were repeated three times and the results matched each other reasonably well. The maximum errors appeared in the three pitch curves; the pitch curve L4 T3 represented the fastest descent speed during the tests.

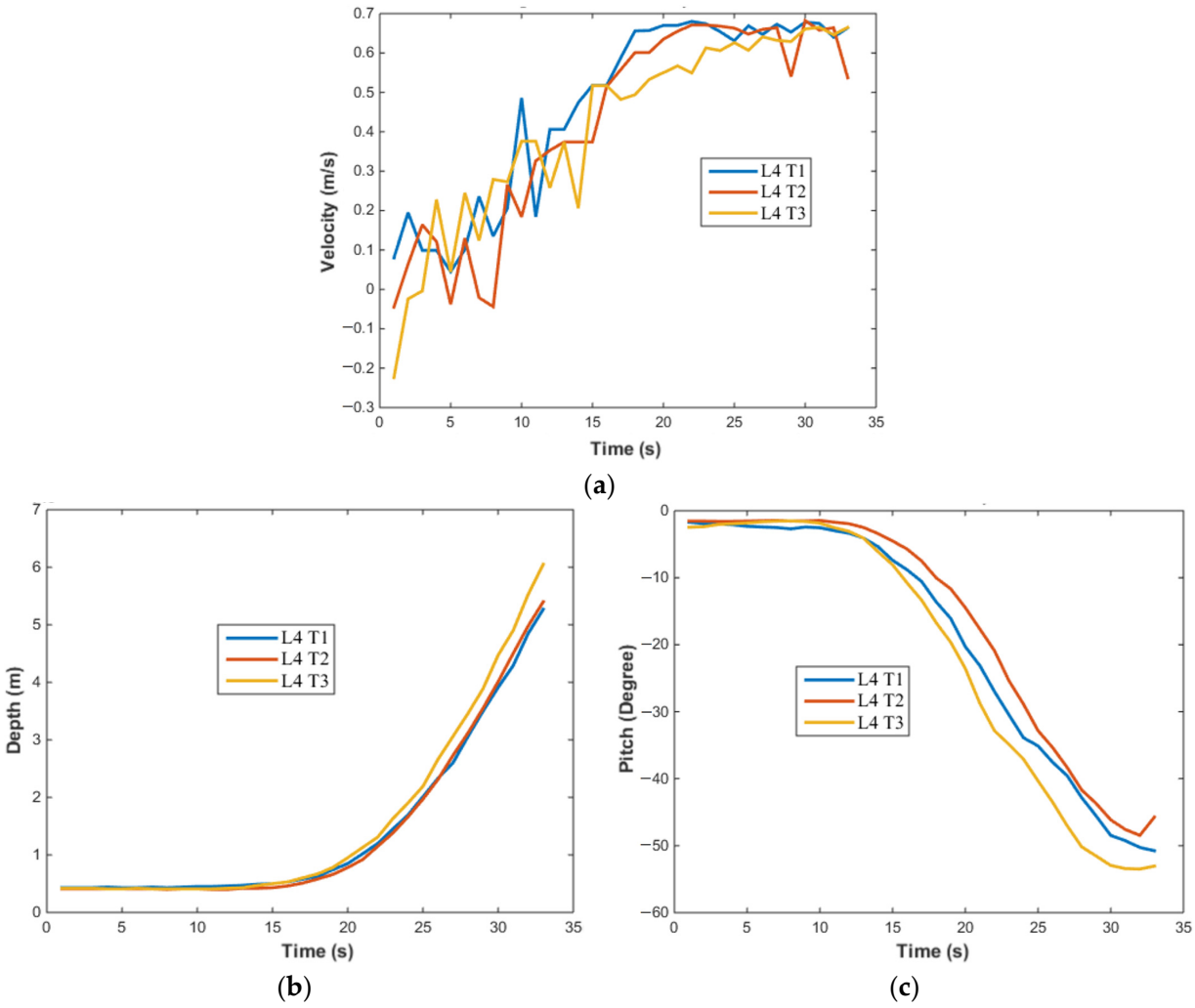

Figure 19. Heave motion of AUV. (**a**) Velocity; (**b**) depth; and (**c**) pitch.

In Figure 19a, the maximum speed along the X-axis was reduced from 0.98 m/s to 0.67 m/s. Figure 19b indicates that, in the initial stage of motion, the depth of the AUV remained unchanged from 0 to 15 s; the depth gradually increased after 15 s, and the descent speed remained stable after 25 s. As shown in Figure 19c, the pitch angle of the AUV remained unchanged from 0 to 12 s, gradually increased after 15 s, and remained stable after 30 s. The maximum pitch angle of the AUV was 53°, and the fastest descent speed of the AUV was 0.45 m/s.

4.1.3. Yaw Motion

The yaw motion of an AUV refers to its rotational movement around the z-axis. The azimuth angle of the vectored thruster was configured to −90 degrees to achieve the highest rate of change in the AUV heading angle. For comparison, the elevator angle was set to its maximum value of 20°. This configuration was intended to induce a counterclockwise rotation in the AUV. Because of the symmetrical shape of the shell of the AUV in the XZ plane, the hydrodynamic characteristics in the counterclockwise and clockwise directions were the same. Simultaneously, the control input to the thrusters was fixed at 4. The test was repeated three times. As shown in Figure 20, the results from the repeated tests matched each other reasonably well. The heading angle of the AUV remained unchanged from 0 s to 12 s and gradually increased after 12 s. The maximum rate of the heading angle was 14.26°/s, and the turning radius was less than 1 m.

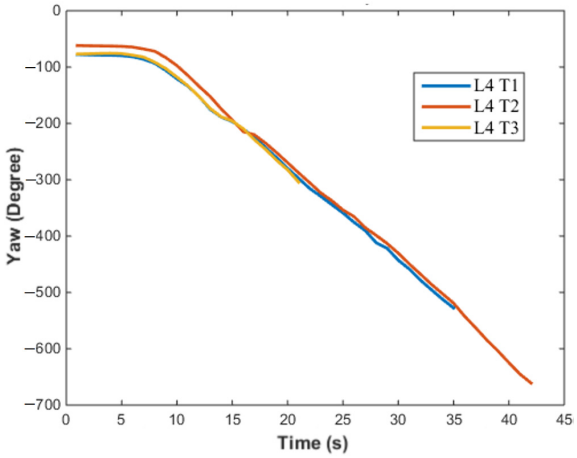

Figure 20. Yaw motion of AUV.

4.2. Offshore Tests

The open-loop test of the vector propeller applied to an AUV was completed in a safe and controllable still-water environment, and the basic performance parameters of the propeller were obtained. Next, a closed-loop test of the AUV's depth and heading control were conducted in an actual marine environment. The test was carried out in Nanshan Port, Sanya City, as shown in Figure 21, and the detailed testing results of offshore depth and heading control can be found in the field test videos provided in the Supplementary Materials.

Figure 21. Offshore testing area of AUV.

The AUV only utilized one vectored thruster, making it an underactuated system. This vectored thruster could only control three degrees of freedom of the AUV, namely speed, depth, and heading direction. The combined force T of the vectored thruster and its three component forces Fx, Fy, and Fz are defined in Equation (10). Specifically, Fx serves as the driving force to control the speed (u) of the AUV, Fy is the steering force for the AUV's

heading direction, and Fz regulates the depth (h) of the AUV. The control scheme of the AUV is shown in Figure 22 below, where all three controllers utilize PID control.

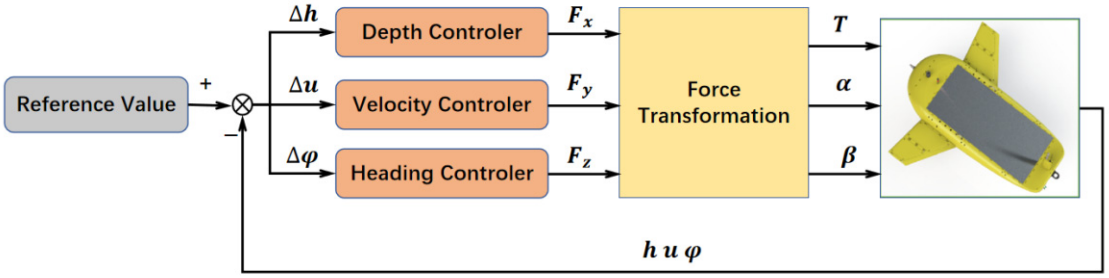

Figure 22. Motion control of AUV.

From Figure 13, we can see that the variation ranges of the three components *Fx*, *Fy*, and *Fz* of the thrust *T* generated by the vectored thruster were [0 112], [−38 38] and [−38 38]. Within these ranges, the control input for the AUV can be calculated using Equation (11) based on the three thrust components $[T \quad \alpha \quad \beta]$.

Generally, the three parameters K_P, K_i, and K_d wee adjusted and set by trial and error. Finally, a set of relatively ideal adjustment parameters were obtained, as shown in Table 6.

Table 6. Coefficients of PID controller.

Parameter	Heading	Depth	Pitch	Velocity
K_P	0.2	1.5	1	1.3
K_i	0.01	0.1	0.1	0.15
K_d	3	5	5	3

During the test, the rotational angular velocity of the linear actuator was set at 1.6°/s, and the rotational angular velocity of the steering motor was set at 25°/s. The target AUV was set with a reference depth of $h_r = 6$ m, a reference speed of $u_r = 0.9$ m/s, and a reference heading of $\varphi_r = 50°$, and multiple tests were conducted. Figure 23 below shows the results of two of these tests.

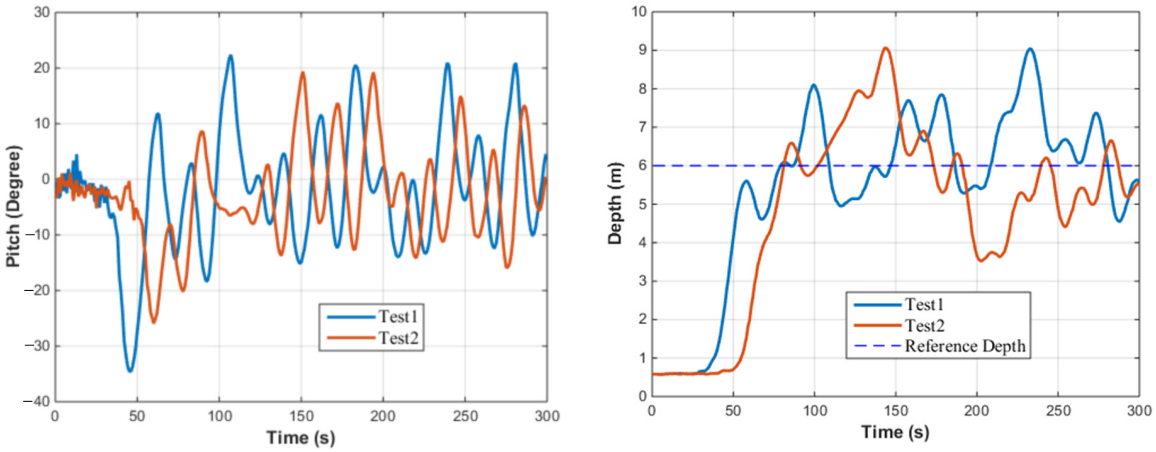

(**a**) (**b**)

Figure 23. *Cont.*

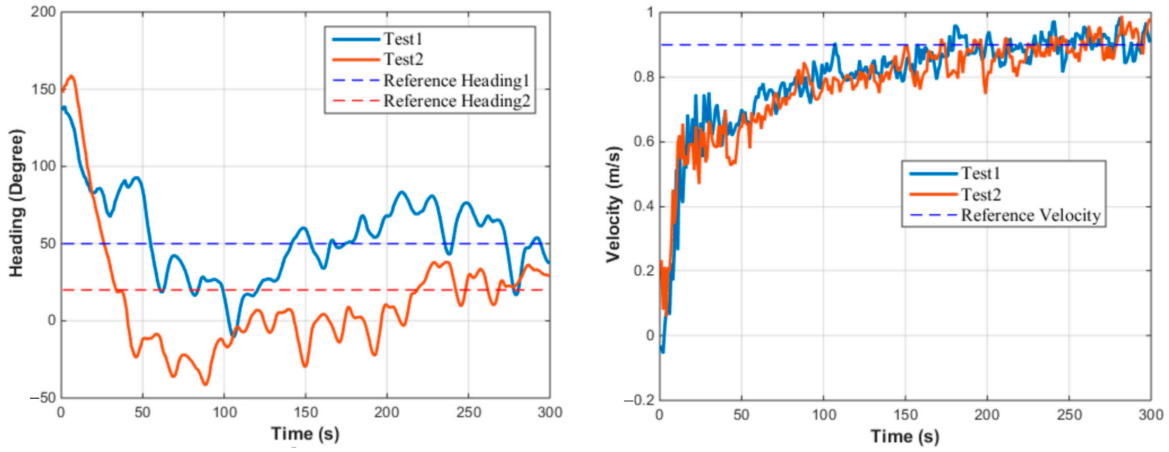

(**c**) (**d**)

Figure 23. Results of motion of AUV (the maximum angular velocity of linear actuator is set at 1.6°/s). (**a**) Pitch; (**b**) depth; (**c**) yaw; and (**d**) velocity.

As can be seen from the diagram, the depth control and heading effect of the AUV based on this vectored thruster were not satisfactory, as the AUV oscillated near the reference values without converging to the target depth and heading. Further discussion is needed on the response of the AUV's steering motor and linear actuator, as illustrated in Figure 24 below.

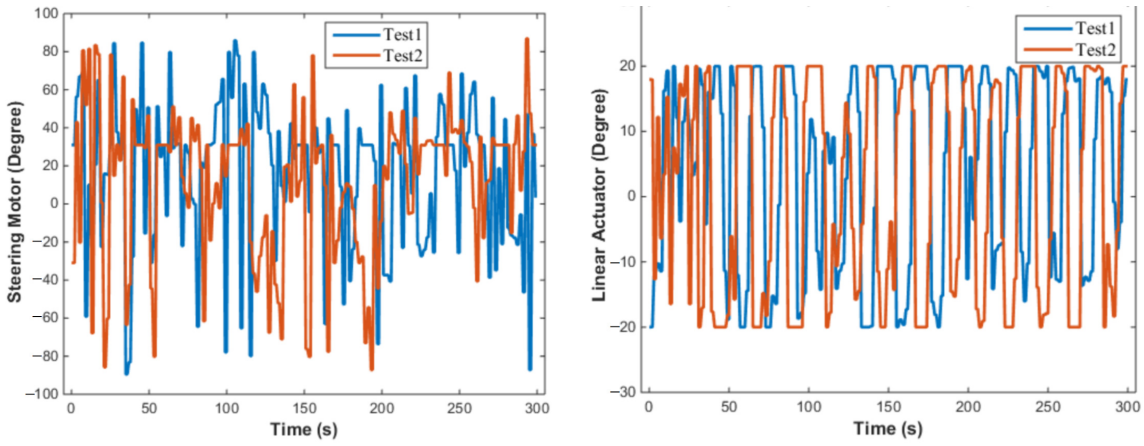

(**a**) (**b**)

Figure 24. The target angle output by the PID. (**a**) Steering motor; (**b**) linear actuator.

Because the depth and heading control did not converged, resulting in repeated oscillations around the reference values, the two actuators needed to continuously adjust the attitude of the vectored thruster based on the PID output. Figure 24 shows the target angle output by the PID, and the linear actuator and the steering motor needed to track this target angle. As seen in Figure 24, the linear actuator would have to adjust from 20° to −20° within 1 s, but with a maximum adjustment angular velocity of 1.6°/s, it was unable to track the target angle output by the PID. Similarly, the steering motor would also need to adjust from 80° to −80° within 1 s, but it was also unable to track the target angle output by the PID. There was a relatively long input delay for the AUV, preventing it from accurately tracking the target depth and heading.

The output angular velocity of the linear actuator needed to be adjusted, and the rotational angular velocity of the linear actuator was reset to 3.2°/s, while the rotational angular velocity of the steering motor was set to 25°/s. With the PID control parameters remaining unchanged, multiple tests were conducted. Figure 25 shows the results of two

tests, where the reference depth of the target AUV was set as $h_r = 6$ m, the reference velocity was $u_r = 1$ m/s, and the reference headings were $\varphi_r = 140°$ and $\varphi_r = 110°$.

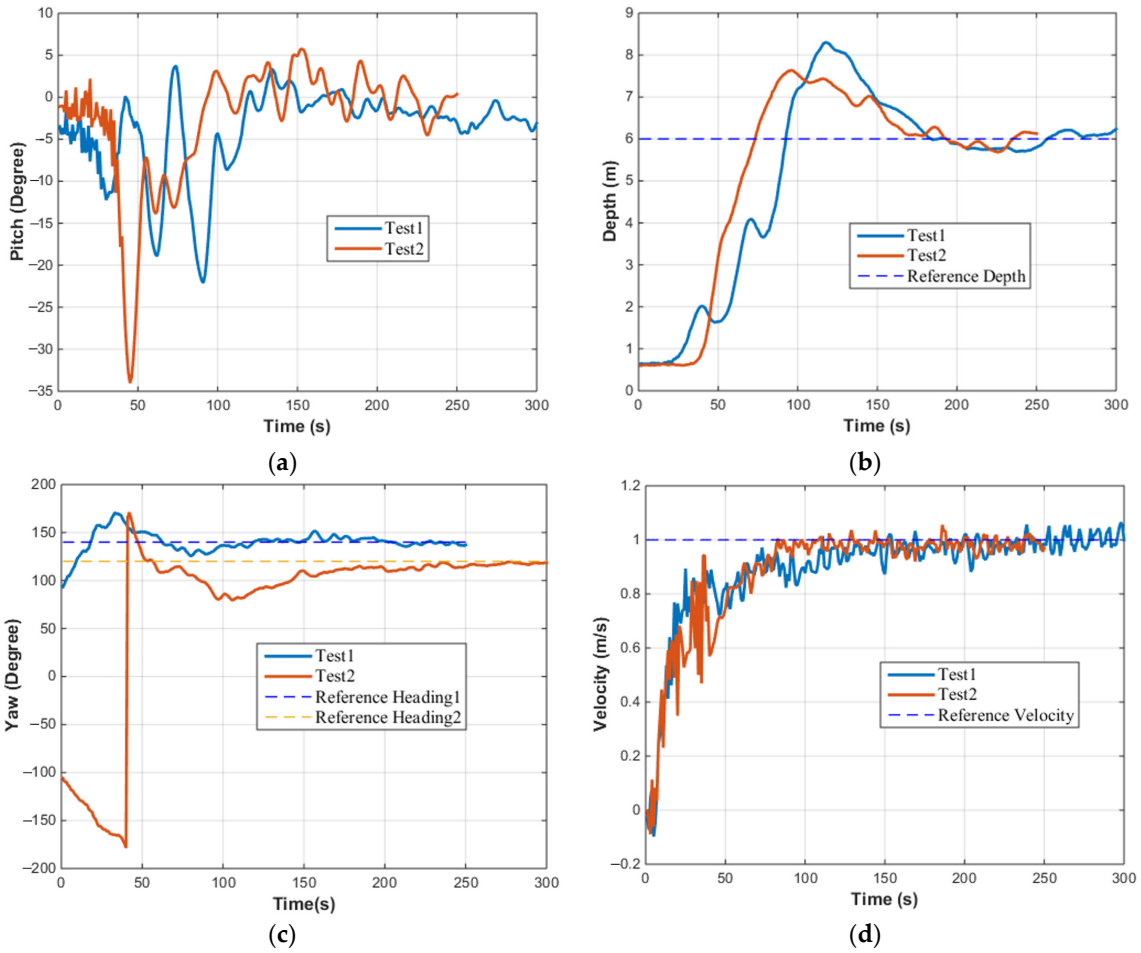

Figure 25. Results of motion of AUV (the maximum angular velocity of linear actuator is set at 3.2°/s). (**a**) Pitch; (**b**) depth; (**c**) yaw; and (**d**) velocity.

From Figure 25, it can be seen that the depth control and heading of the AUV based on this vectored thruster achieved the expected results, both converging to the reference values. The response of the steering motor and linear actuator is also presented in Figure 26.

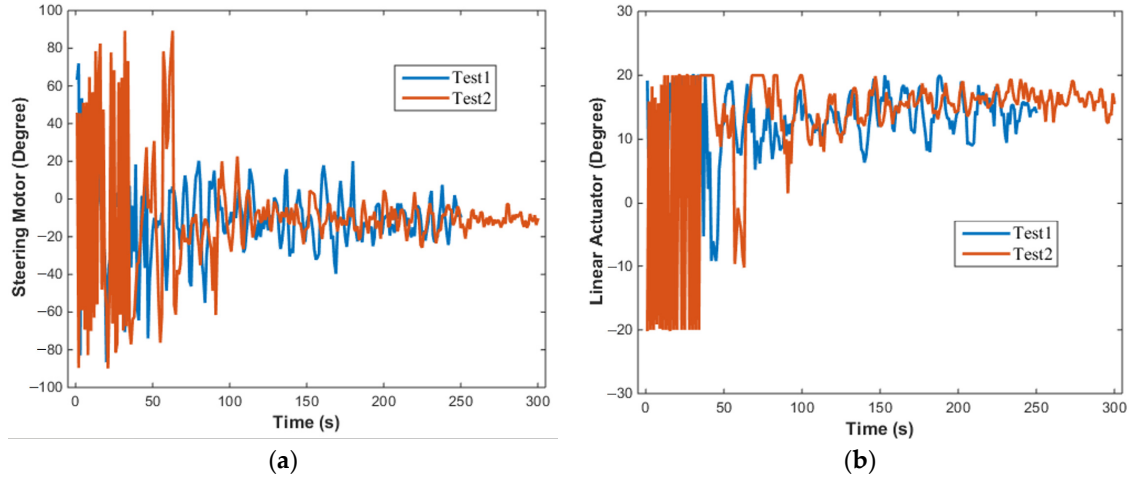

Figure 26. Yaw motion of AUV. (**a**) Steering motor; (**b**) linear actuator.

As seen in Figure 26, during the first 40 s, there was a significant error between the actual pitch angle and heading angle when compared to the reference values. The range of target angle variations output by the PID was relatively wide, making it difficult for the linear actuator and the steering motor to track the target angle. However, after 40 s, the error between the actual pitch and heading angles and their reference values gradually decreased, allowing the linear actuator and the steering motor to track the target angle output by the PID. As the movement of the AUV stabilized, the adjustment range of the linear actuator and the actuator's output gradually narrowed, eventually reaching a stable state. This indicates that when the rotational angular velocity of the linear actuator is set to 3.2°/s and the rotational angular velocity of the steering motor is set to 25°/s, the configured vectored thruster can meet the AUV's motion control requirements. In future research, a more suitable controller can be designed for this vectored thruster to further enhance the stability of the AUV's motion control.

5. Conclusions

In this study, we designed a vectored thruster based on a linear actuator and steering motor to satisfy the design requirements of a specially shaped AUV. It employs a ductless propeller as a thrust supply to produce a vectored thrust for driving the AUV. Propulsive force tests were performed to evaluate its performance. Kinematic analyses of the thrust-vectoring mechanism were performed to achieve reliable and accurate control of the thrust-vectoring mechanism.

An AUV equipped with the designed vectored thruster was built to verify the design principles. The AUV was tested in a water tank. The thrust used for propelling and controlling the AUV was selected to study the vehicle's response at various vectoring angles.

Three basic motions (surge, pitch, and yaw) of an AUV are essential and efficient methods for evaluating the propulsive efficiency of a newly developed vectored thruster. The results showed that the thrust-vectoring mechanism directionally regulates vectored thrust. The vectored thruster can reach a sufficient level for AUV control.

The performance of the vectored thrusters in actual marine environments was tested, indicating that the vectored thrusters can meet the motion control requirements of AUVs. In the future, long-term sea trials will be conducted on the AUV to verify the durability and reliability of the vectored thruster. Considering the characteristics of the vectored thruster from the perspective of control algorithms, such as the rate and range of variation in the elevation angle α, the motion control of the AUV can be more efficient. In addition, in subsequent tests, improvements and upgrades will be made to the vectored thruster based on the problems encountered.

Supplementary Materials: The following supporting information can be downloaded at: https://www.mdpi.com/article/10.3390/act13060228/s1. This section provides videos of field tests, including the open-loop control test video in the water tank, and the offshore heading control test video and depth control test video to demonstrate the effectiveness and mechanism of the work.

Author Contributions: We confirm that the authors mentioned in the manuscript have been approved as the sole contributors and authors. We confirm that the manuscript has been read and approved by the authors and that there are no other persons who satisfied the criteria for authorship. All authors agree to be accountable for all aspects of the work. The main contributions of the authors are as follows: H.Z. designed the mechanical structure of the vectored thruster. L.L. drafted the manuscript and reviewed it critically. C.Y. provided the software implementation strategy for the vectored thruster. Y.C. agreed to be accountable for all aspects of the work in ensuring that questions related to the accuracy or integrity of any part of the work are appropriately investigated and resolved. H.X. completed the design and optimization of the blades. Y.X. completed the experiments mentioned in the manuscript. G.Z. provided the hardware implementation strategy for the vectored thruster. All authors have read and agreed to the published version of the manuscript.

Funding: The research was supported by the Hainan Provincial Joint Project of Sanya Yazhou Bay Science and Technology City (No. 2021CXLH0003) as well as Sanya Science, Technology, Industry and Information Technology Bureau (No. 2022KJCX65).

Data Availability Statement: The data that support the findings of this study are available from the corresponding author, Chen Yuxiang, upon reasonable request.

Acknowledgments: We wish to express our heartfelt appreciation to our research institutes. Their unwavering support, intelligent recommendations, and vital resources were critical to completing this research on the design and application of a novel vectored thruster for a specially shaped AUV. We are excited to investigate the possibilities of our unique vectored thruster for specially shaped autonomous underwater vehicles and to contribute to the growth of maritime technology.

Conflicts of Interest: The authors declare no conflict of interest.

References

1. Fagundes Gasparoto, H.; Chocron, O.; Benbouzid, M.; Siqueira Meirelles, P. Advances in Reconfigurable Vectorial Thrusters for Adaptive Underwater Robots. *J. Mar. Sci. Eng.* **2021**, *9*, 170. [CrossRef]
2. Liu, T.; Hu, Y.; Xu, H.; Wang, Q.; Du, W. A Novel Vectored Thruster Based on 3-RPS Parallel Manipulator for Autonomous Underwater Vehicles. *Mech. Mach. Theory* **2019**, *133*, 646–672. [CrossRef]
3. Li, Y.; Tian, C.; Wang, Y.; Gao, P.; Ma, X. Design and Simulation of a Collaborative Propulsion System for the Underwater Robot. *Int. J. Robot. Eng.* **2019**, *4*, 1–19.
4. Li, Y.; Guo, S.; Wang, Y. Design and Characteristics Evaluation of a Novel Spherical Underwater Robot. *Robot. Auton. Syst.* **2017**, *94*, 61–74. [CrossRef]
5. Kadiyam, J.; Mohan, S. Conceptual Design of a Hybrid Propulsion Underwater Robotic Vehicle with Different Propulsion Systems for Ocean Observations. *Ocean Eng.* **2019**, *182*, 112–125. [CrossRef]
6. Hu, H.; Wang, Y. Vertical Force Generation of a Vectorial Thruster That Employs a Rigid Flapping Panel. *Phys. Fluids* **2021**, *33*, 061906. [CrossRef]
7. Liu, T.; Hu, Y.; Xu, H.; Zhang, Z.; Li, H. Investigation of the Vectored Thruster AUVs Based on 3SPS-S Parallel Manipulator. *Appl. Ocean Res.* **2019**, *85*, 151–161. [CrossRef]
8. Pugi, L.; Allotta, B.; Pagliai, M. Redundant and Reconfigurable Propulsion Systems to Improve Motion Capability of Underwater Vehicles. *Ocean Eng.* **2018**, *148*, 376–385. [CrossRef]
9. Kadiyam, J.; Mohan, S.; Deshmukh, D. Control of a Vectorial Propulsion Underwater Vehicle Considering Thruster Hydrodynamics Constraints and Actuator Saturation. In Proceedings of the Global Oceans 2020: Singapore–US Gulf Coast, Biloxi, MS, USA, 5–30 October 2020; pp. 1–10.
10. Kadiyam, J.; Mohan, S.; Deshmukh, D.; Seo, T. Simulation-Based Semi-Empirical Comparative Study of Fixed and Vectored Thruster Configurations for an Underwater Vehicle. *Ocean Eng.* **2021**, *234*, 109231. [CrossRef]
11. Lin, X.; Guo, S. Development of a Spherical Underwater Robot Equipped with Multiple Vectored Water-Jet-Based Thrusters. *J. Intell. Robot. Syst.* **2012**, *67*, 307–321. [CrossRef]
12. Kopman, V.; Cavaliere, N.; Porfiri, M. A Thrust-Vectored Submersible for Animal Behavior Research: Design and Proof of Concept. In Proceedings of the ASME 2010 Dynamic Systems and Control Conference, DSCC2010, Cambridge, MA, USA, 12–15 September 2010; Volume 1.
13. Cavallo, E.; Michelini, R.C.; Filaretov, V.F. Conceptual Design of an AUV Equipped with a Three Degrees of Freedom Vectored Thruster. *J. Intell. Robot. Syst.* **2004**, *39*, 365–391. [CrossRef]
14. Cavallo, E.; Michelini, R.C. A Robotic Equipment for the Guidance of a Vectored Thurstor AUV. In Proceedings of the 35th International Symposium on Robotics ISR, Paris, France, 23–26 March 2004.
15. Guo, S.; Lin, X.; Tanaka, K.; Hata, S. Modeling of Water-Jet Propeller for Underwater Vehicles. In Proceedings of the 2010 IEEE International Conference on Automation and Logistics, Hong Kong, China, 16–20 August 2010; pp. 92–97.
16. Chocron, O.; Prieur, U.; Pino, L. A Validated Feasibility Prototype for AUV Reconfigurable Magnetic Coupling Thruster. *IEEE/ASME Trans. Mechatron.* **2013**, *19*, 642–650. [CrossRef]
17. Gao, F.; Han, Y.; Wang, H.; Ji, G. Innovative Design and Motion Mechanism Analysis for a Multi-Moving State Autonomous Underwater Vehicles. *J. Cent. South Univ.* **2017**, *24*, 1133–1143. [CrossRef]
18. Papachristos, C.; Alexis, K.; Tzes, A. Efficient Force Exertion for Aerial Robotic Manipulation: Exploiting the Thrust-Vectoring Authority of a Tri-Tiltrotor UAV. In Proceedings of the 2014 IEEE International Conference on Robotics and Automation (ICRA), Hong Kong, China, 31 May–7 June 2014.
19. Gucer, Ç.A.; Onur, A.; Kantarcioglu, B.; Cenk, U. Thruster Design for Unmanned Underwater Vehicles. *Selçuk-Tek. Derg.* **2020**, *19*, 196–208.
20. Darmawan, S.; Raynaldo, K.; Halim, A. Investigation of Thruster Design to Obtain the Optimum Thrust for Rov (Remotely Operated Vehicle) Using CFD. *Evergreen* **2022**, *9*, 115–125. [CrossRef]
21. Atalı, G. Prototyping of a Novel Thruster for Underwater ROVs. *Int. J. Appl. Math. Electron. Comput.* **2022**, *10*, 11–14. [CrossRef]

22. Laidani, A.; Bouhamida, M.; Benghanem, M.; Sammut, K.; Clement, B. A Low-Cost Test Bench for Underwater Thruster Identification. *IFAC-PapersOnLine* **2019**, *52*, 254–259. [CrossRef]
23. Li, C.; Guo, S.; Guo, J. Performance Evaluation of a Hybrid Thruster for Spherical Underwater Robots. *IEEE Trans. Instrum. Meas.* **2022**, *71*, 7503110. [CrossRef]